Supporting Information

Dynamic Ferroelectric Transistor-based Reservoir Computing for Spatiotemporal Information Processing

*Ngoc Thanh Duong, Yu-Chieh Chien, Heng Xiang, Sifan Li, Haofei Zheng, Yufei Shi, and Kah-Wee Ang**

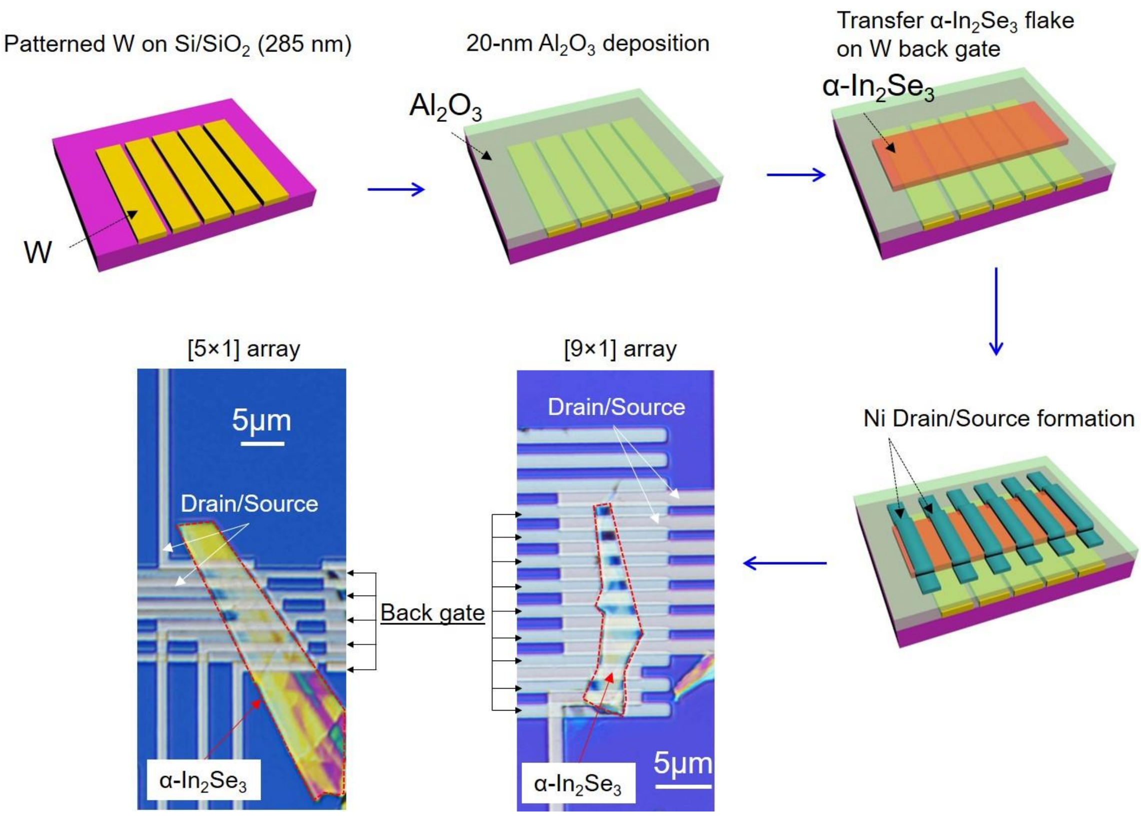

Figure S1. 1D array fabrication techniques and optical images of [5×1] and [9×1] array.

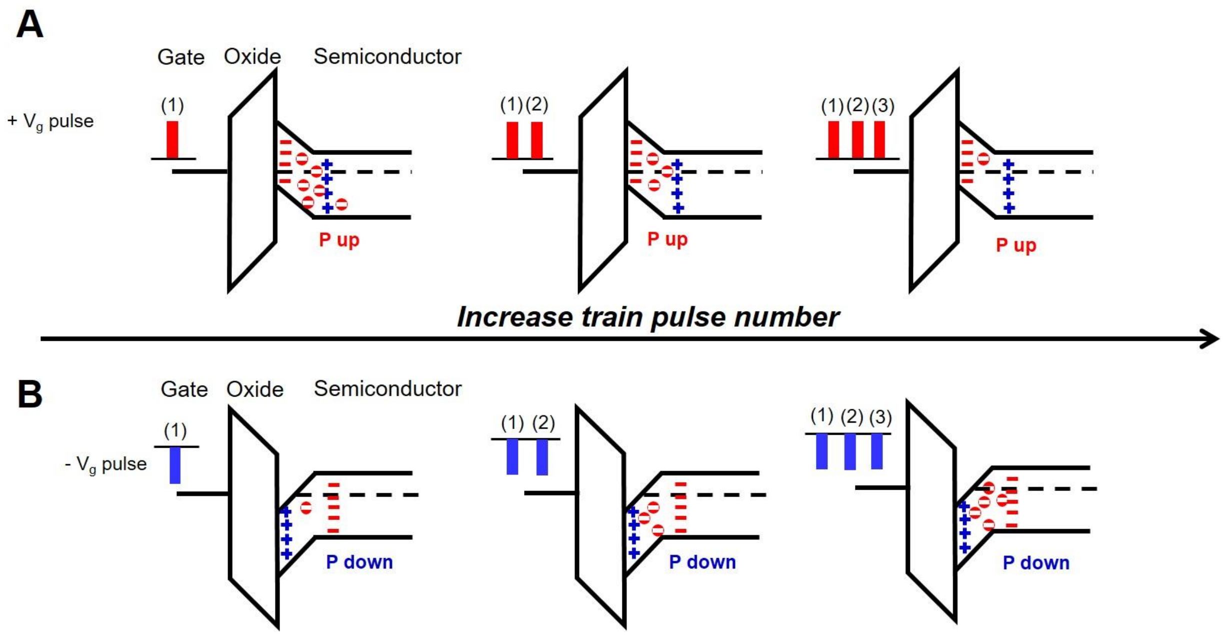

Figure S2. Band alignment showing charge distribution at two polarization direction in α-In-$_2$Se$_3$ which explain for the change in channel conductance after applying series discrete (a) positive and (b) negative V_g pulses.

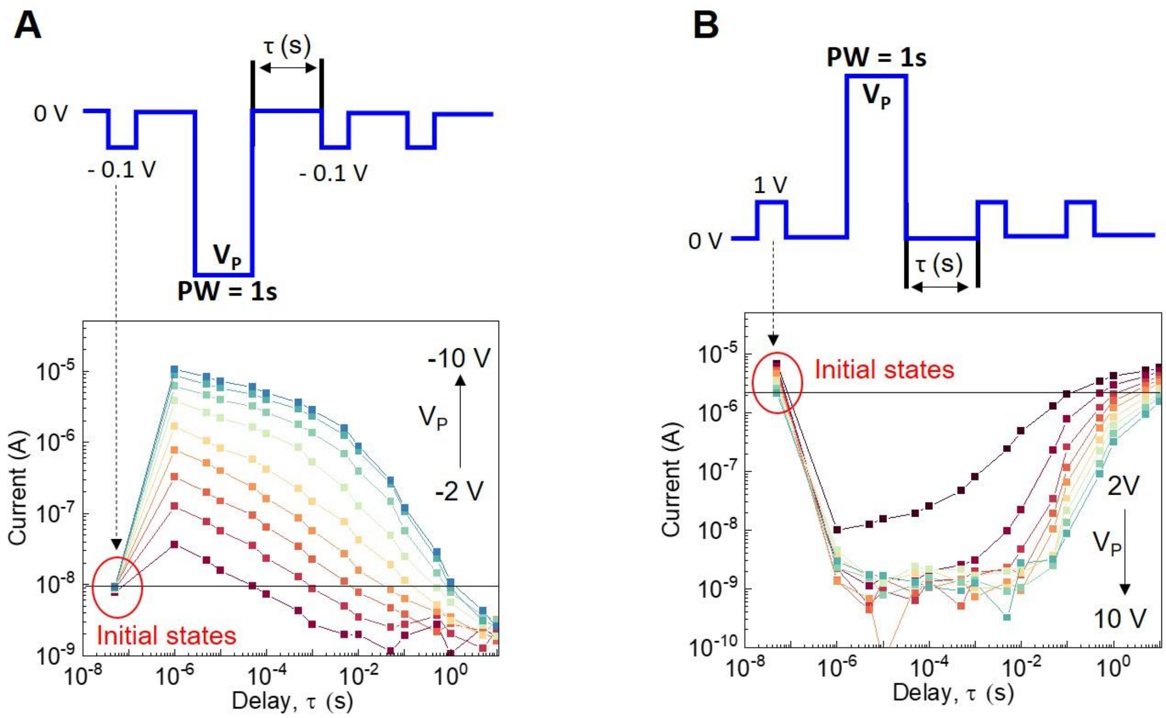

Figure S3. Drain currents read at various delay time τ (s) after writing by (**A**) negative and erasing by (**B**) positive V_p. In both regimes, the conductances retrieved their initial states after a very short time delay (< 1 s).

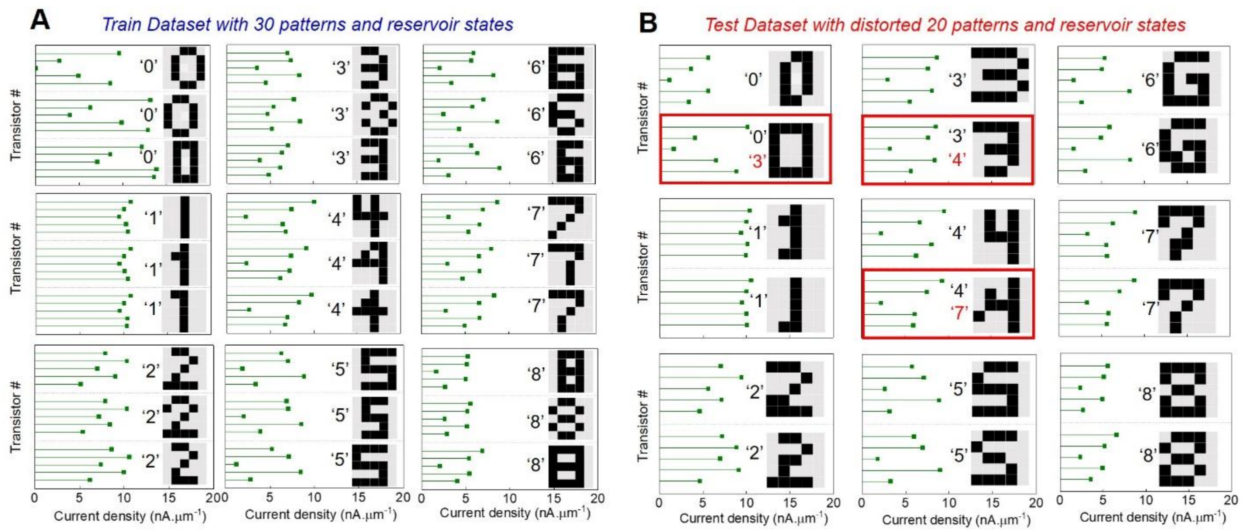

Figure S4. Dataset for pattern recognition (a) 30 images traning dataset showing different digits with corresponding reservoir states experimentally measured by [5×1] transistor array. (b) 20 distorted images for testing with purposely created noises by adding or deleting random fixels. Red-marked three wrongly predicted digit ‘0’, ‘3’, and ‘4’.

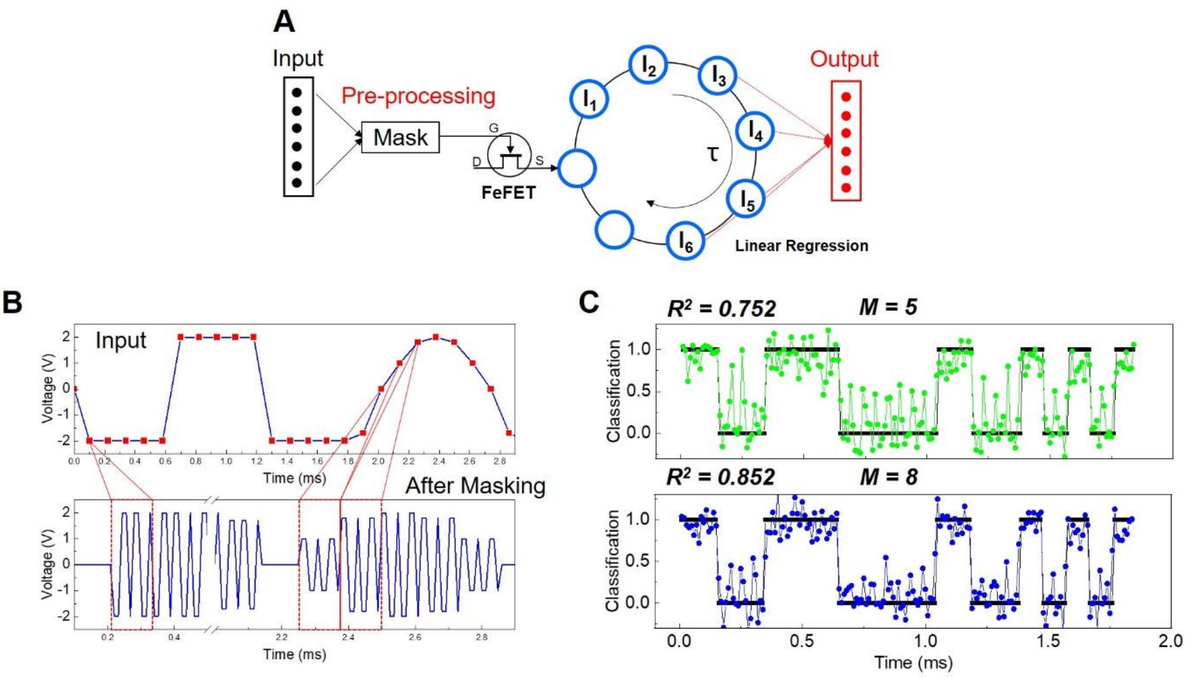

Figure S5. Waveform classification task. (a) Concept of cyclic reservoir in which input data is time-multiplxed by a masking process to create the sequential input voltages. Next, the input voltages stream in (b) is then applied to our α-In_2Se_3 FeS-FET to record to virtual nodes in reservoir space. The virtual nodes are connected to each other by a time sequence. The number of virtual nodes are decided by the mask length, M. The virtual node are then sent to readout layer with simple linear regression. (c) The classification results and R^2 with increasing mask length, M = 5 and 8.

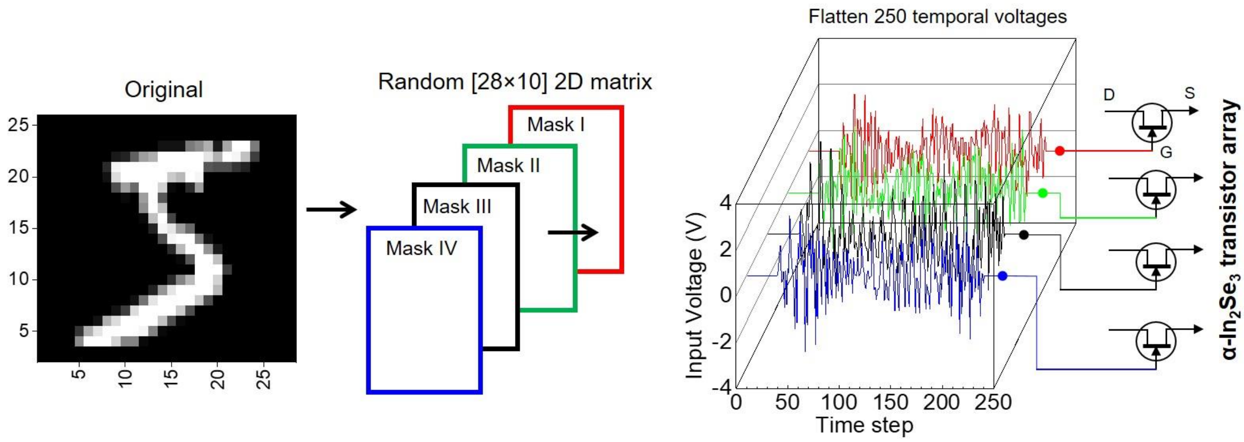

Figure S6. Image in MNIST database is pre-processed by multiplying with 2D mask [28×10] to generated temporal input voltage, V (t) with time delay τ = 120 µs. The V (t) is then streamed through a 1D array of devices to sense conductance states (virtual nodes) for further training and testing.

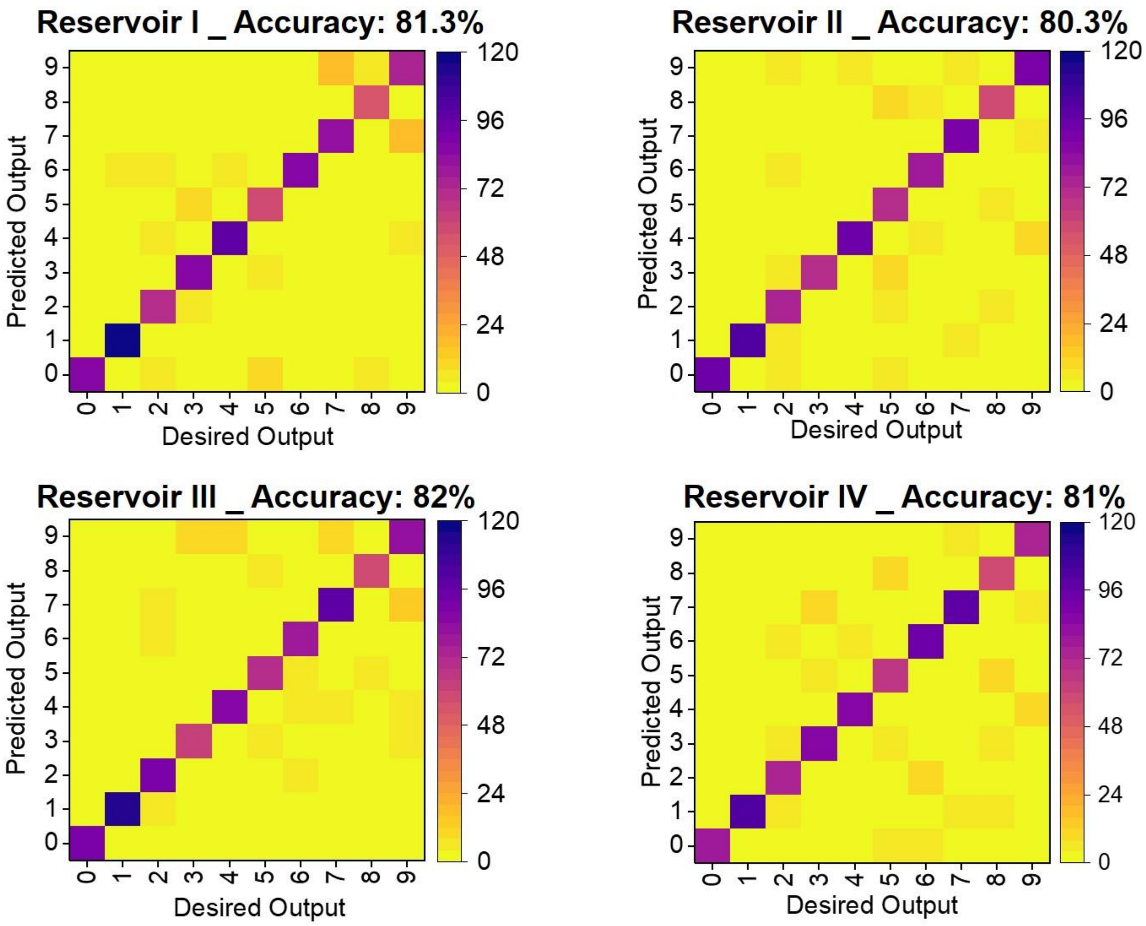

Figure S7. Detail confusion matrices for 4 different reservoirs as shown in Fig. 4 B

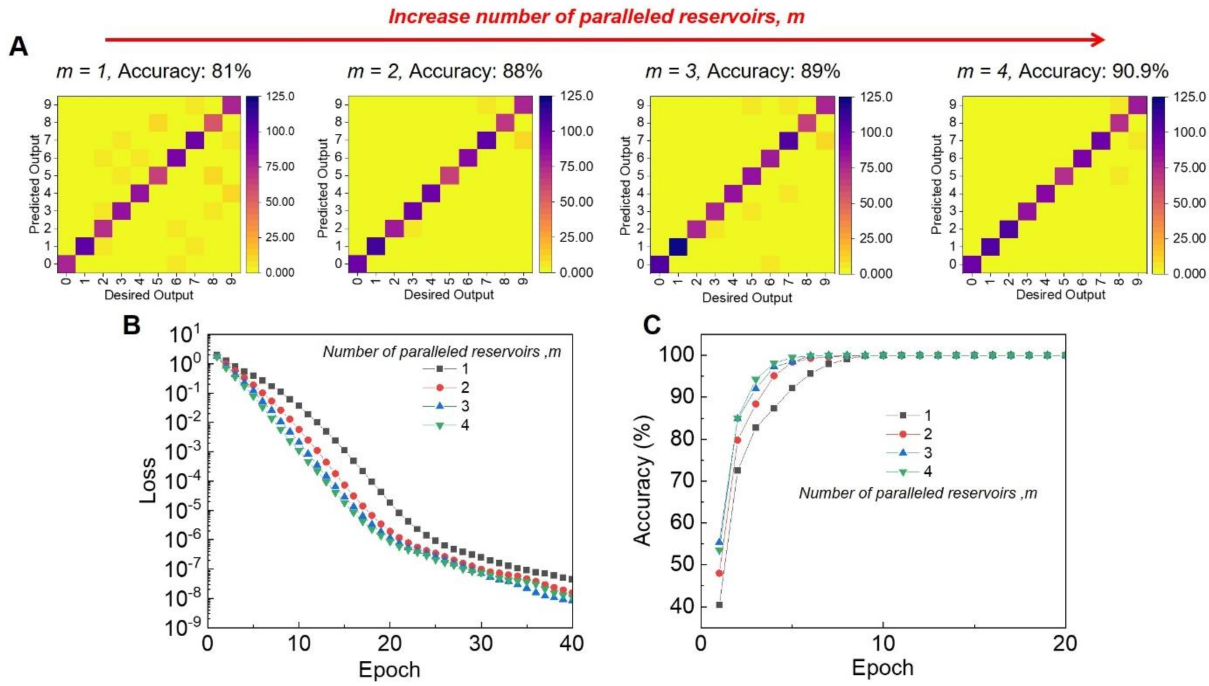

Figure S8. (a) Confusion matrices of testing, (b) Loss and (c) Accuracy versus training epoch process with increasing number of paralleled reservoirs, m

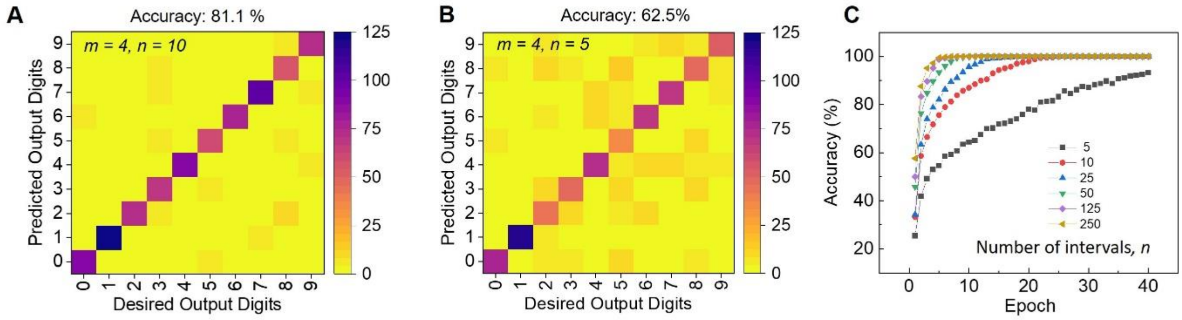

Figure S9. Confusion matrices at with 4 paralleled reservoirs, $m = 4$ at different input selection intervals: (a) n =10 and (b) n = 5 showing accuracy = 81.1 % and 62.5 %, respectively. (c) Accuracy *versus* 40 training epoch with increase number of selected virtual nodes, n

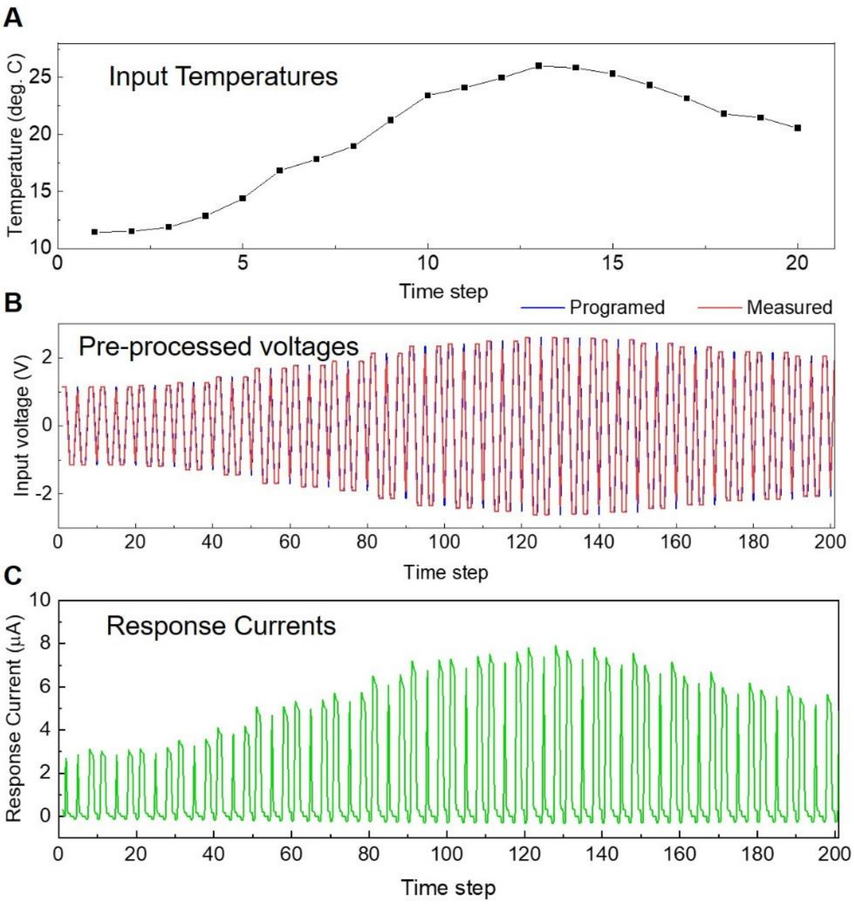

Figure S10. (a) Time-series daily temperature serves as input layer in RC systems. (**b**) Programmed and measured time-multiplexed input voltages after masking the input temperature in figure S10 a. (**C**) Response currents of FeS-FET utilized as virtual nodes for readout function.

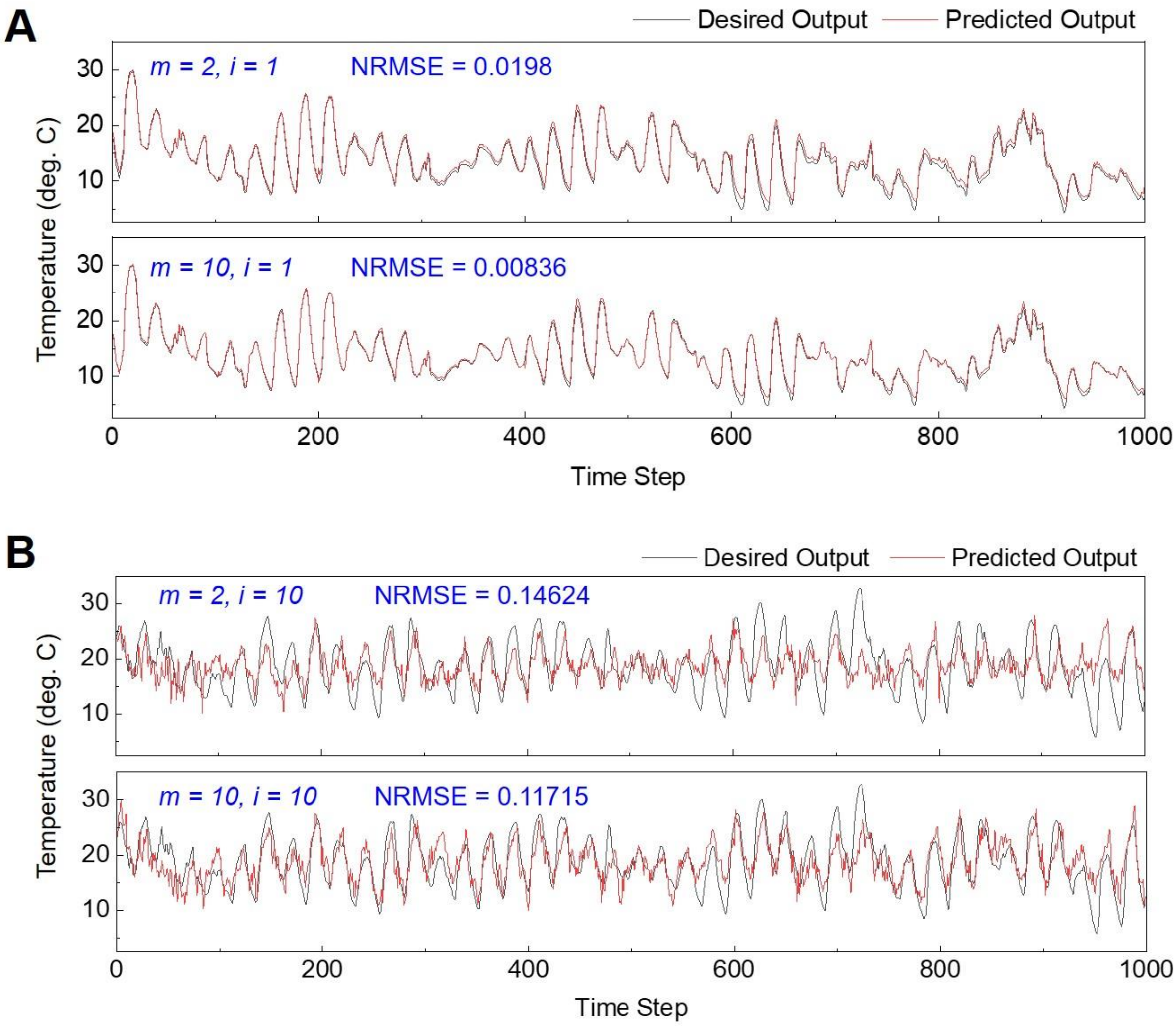

Figure S11. Visualization of predicted and desired output for 1000 testing dataset and their compromised NRMSE at some steps prediction ahead, i: (a) i =1 and (b) i = 10 with m = 2 and 10.

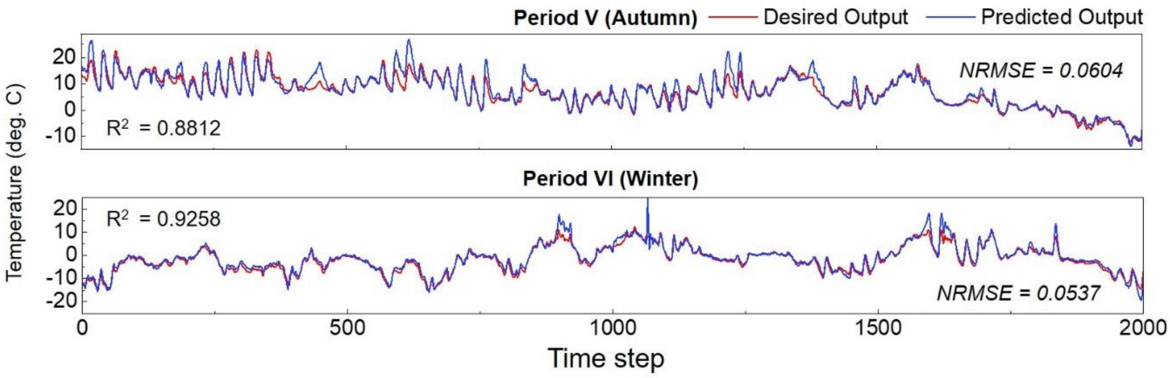

Figure S12. Desired and predicted output for testing period V (Autumn) and VI (Winter) and its coresponding R^2 and NRMSE.

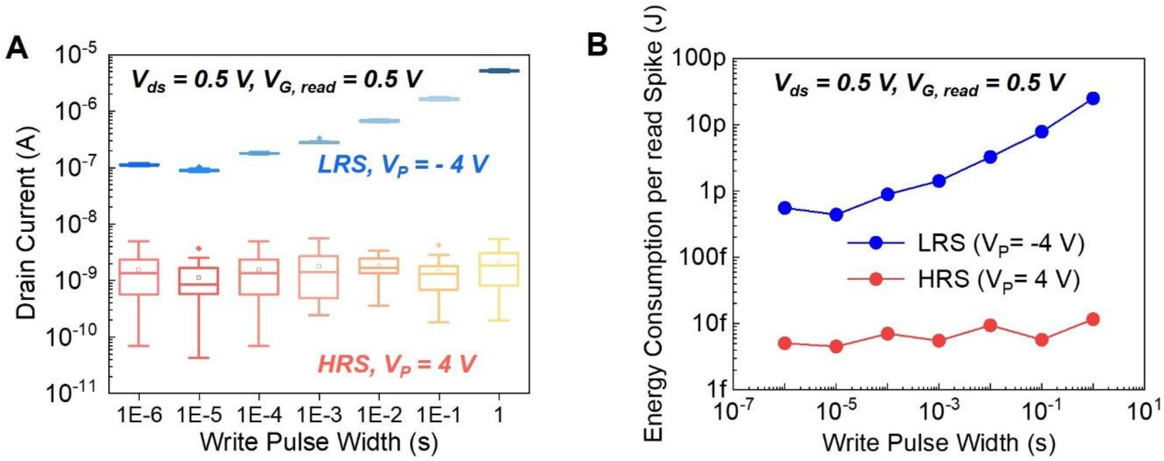

Figure S13. (a) Resistive switching with different writing speeds. LRS/HRS ratio increases with the increase of writing widths. (b) Power consumption within a reading spike (0.5 V, 20 µs) of our fading Ferro RC versus writing speed.